 CMES, vol.64, no.3, pp.299-326, 2010

An Iterative and Adaptive Lie-Group Method for Solving the Calderón Inverse Problem

Chein-Shan Liu[1] **and Satya N. Atluri**[2]

Abstract: We solve the Calderón inverse conductivity problem [Calderón (1980, 2006)], for an elliptic type equation in a rectangular plane domain, to recover an unknown conductivity function inside the domain, from the over-specified Cauchy data on the bottom of the rectangle. The Calderón inverse problem exhibits *three-fold simultaneous difficulties: ill-posedness of the inverse Cauchy problem, ill-posedness of the parameter identification, and no information inside the domain being available on the impedance function*. In order to solve this problem, we discretize the whole domain into many sub-domains of finite strips, each with a small height. Thus the Calderón inverse problem is reduced to an inverse Cauchy problem and a parameter identification problem in each finite strip. An effective combination of the Lie-group adaptive method (LGAM), together with a finite-strip method is developed, where the Lie-group equation can adaptively solve the semi-discretized ODEs to find the unknown conductivity coefficients through iterations. The success of the present method hinges on a rationale that *the local ODEs and the global Lie-group equation have to be self-adaptive during the iteration process*. Thus, we have a computationally inexpensive mathematical algorithm to solve the Calderón inverse problem. The feasibility, accuracy and efficiency of present method are evaluated by comparing the estimated results for the unknown impedance function in the domain, in the Calderón inverse problem, with some postulated exact solutions. It may be concluded that the iterative and adaptive Lie-group method presented in this paper, may provide a simple and effective means of solving the Calderón inverse problem in general domains.

Keywords: Calderón's inverse problem, Inverse Cauchy problem, Parameter identification problem, Lie-group adaptive method, Iterative method

[1] Department of Civil Engineering, National Taiwan University, Taipei, Taiwan. E-mail: liucs@ntu.edu.tw

[2] Center for Aerospace Research & Education, University of California, Irvine

1 Calderón's inverse problems [Calderón (1980, 2006)]

The electrical impedance tomography (EIT) is a diffuse imaging process, in which the resistivity inside the body is estimated by electrical measurements of the current and the potential taken on the boundary. In a similar context, Kaup, Santosa and Vogelius (1996) have modeled the effects of material losses due to corrosion, and then, Santosa, Vogelius and Xu (1999) related the effects of damage to the impedance condition.

Corrosion of metals may change the impedance coefficient, and thus induces an unknown Robin [or impedance] condition in the inaccessible part of the body. Identifying the impedance coefficient may be an effective way to find the location of corrosion, and one may possibly assess the level of corrosion according to the exterior measurements, and then using the solution of the inverse problem by the EIT. In a simpler corrosion model, the Robin coefficient quantifies the level of corrosion of some inaccessible part of the boundary [Liu (2009a)]. The model problem was to recover the Robin coefficient by means of the current flux and potential measurements on a partialy accessible boundary in a finite annulus.

The computerized tomography is by now a standard tool in medical diagonstics and non-destructive testing of materials. Besides the well-established methods of X-ray and MRI, the last three decades have witnessed an increasing interest in the new imaging technique of EIT, due to its easy implementation and low cost. A comprehensive review of EIT was given by Borcea (2002). *In EIT, the electrical conductivity distribution inside an object is determined from measurements of currents and voltages on the surface of the object*.

Calderón (1980) was the first to coin the phrase of an inverse boundary value problem for studying the EIT technique by mathematical modeling, since the conductivity appears as a variable coefficient of diffusion in an elliptic partial differential equation. In fact it is an inverse problem of the Neumann to Dirichlet mapping by knowing the voltage and current on the boundary. There have been numerous papers in the mathematical and engineering literature addressing such diverse topics as the identifiability and stability of solutions for conductivity, the design of measurement devices, mathematical modeling of electrodes, and methods of numerical reconstruction: to name a few, Adler and Guardo (1994), Borcea, Gray and Zhang (2003), Brown and Uhlmann (1997), Francini (2000), Knowles (1998), Kohn and McKenney (1990), Levy, Adam and Bresler (2002), Meeson, Killingback and Blott (1995), Murai and Kagawa (1985), Nachman (1988, 1996), Siltanen, Mueller and Isaacson (2000), Stasiak, Sikora, Filipowicz and Nita (2007), Sylvester and Uhlmann (1987), Wexler, Fry and Neuman (1985), Yorkey, Webster and Tompkins (1987), Zlochiver, Rosenfeld and Abboud (2003), and Zadehkoochak, Hames

and Blott (1990). In this paper we attempt to approach this difficult inverse problem of numerical reconstruction of the conductivity function in the interior of a domain, by reformulating the Lie-group shooting method in its more general versions.

More specifically, we consider a computational modeling of this problem, and give an effective numerical algorithm to infer the conductivity function inside the body by measuring an electrical field on the boundary. Given the Cauchy data on $u(x,y)$ *and* $\partial u/\partial n(x,y)$ at the point $(x,y) \in \mathbb{R}^2$ with an unit outward normal $n(x,y)$ on the boundary Γ of a simply connected domain Ω, we consider Calderón's model inverse problem [Calderón (1980, 2006)] of finding $\sigma(x,y)$ from the following equations:

$$\nabla \cdot (\sigma \nabla u) = h, \quad (x,y) \in \Omega, \tag{1}$$

$$u(\rho,\theta) = h_1(\theta), \quad 0 \le \theta \le 2\pi, \tag{2}$$

$$u_n(\rho,\theta) = h_2(\theta), \quad 0 \le \theta \le 2\pi, \tag{3}$$

where $h(x,y)$ is specified in Ω, $h_1(\theta)$ and $h_2(\theta)$ are the specified Cauchy data on the boundary, ∇ is the gradient operator, and $\sigma(x,y)$ is to be determined. Specifically, the presently considered Calderón inverse problem is defined as follows:

The presently solved inverse problem: *Find the unknown function* $\sigma(x,y)$ *in the interior of a rectangular domain* $\Omega := \{(x,y) \mid 0 \le x \le \ell_x,\ 0 \le y \le \ell_y\}$ *under an over-specified Cauchy set of data on the bottom of* Ω*, and the function* $\sigma(x,y)$ *on the left- and right-boundary of* Ω *are known, as shown in Fig. 1.*

This paper is organized as follows. In Section 2 we describe a "finite-strip" method,

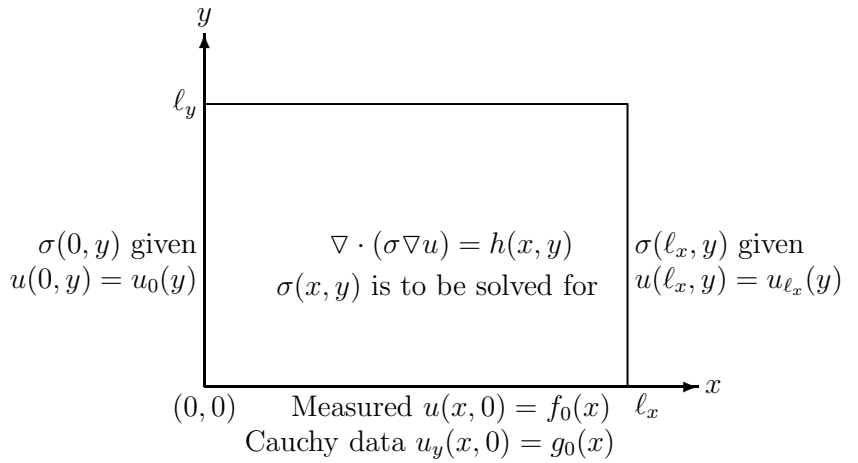

Figure 1: A schematic diagram of the presently solved Calderón inverse problem of identifying $\sigma(x,y)$ inside a rectangle.

wherein a generic j-th strip of finite thickness in the y-direction, $y_j \le y \le y_{j+1}$, is considered, and $\sigma(x,y_j) = \sigma^j(x)$ [σ is a function of x alone] is assumed to be approximately valid. Section 3 gives a semi-discretization method in the j-th strip whereby the governing PDE in (x,y) is reduced to *a system of ODEs* in y alone. Section 4 deals with the numerical solution of the ODEs derived in Section 3, through developing a Lie-group formulation, including a group-preserving scheme for the inverse Cauchy problem along each line (x_i,y), a one-step Lie-group transformation, and a two-point Lie-group equation. The Lie-group method is described in Section 5. In Section 6, we enhance the Lie-group shooting method to be a Lie-group adaptive method, which is suitable for the estimation of an unknown parameter, without having a real target. In Section 6 the numerical procedures are also described. The numerical verifications with four numerical examples are carried out in Section 7. Finally, some significiant conclusions are drawn in Section 8.

2 The present finite strip method

In order to treat the Calderón inverse problem in a rectangular domain $\Omega := \{(x,y) \mid 0 \le x \le \ell_x,\ 0 \le y \le \ell_y\}$, we divide the 2-D domain into m strips along the y-direction, and $\sigma(x,y)$ in the j-th strip is approximated by $\sigma(x,y_j) = \sigma^j(x)$, which is viewed as a function only of x. The domain Ω is now decomposed into m subdomains of $\Omega = \cup_{j=1}^{j=m}\Omega_j$ with $\Omega_j = \{(x,y) \mid 0 \le x \le \ell_x,\ y_j \le y \le y_{j+1}\}$ where $y_j = (j-1)\delta y = (j-1)\ell_y/m$, and we can simplify the above elliptic equation (1) defined in a whole domain into that defined in each finite strip, and solve an inverse Cauchy problem as well as a parameter identification problem in each strip, based on the data calculated from the $(j-1)$-th strip. In Fig. 2 we give a schematic plot to show the above idea. Therefore, the solution of the original Calderón inverse problem is obatined by piecing together all the solutions obtained in each strip.

Now, the equations in the j-th strip can be simplified to

$$\sigma'(x)\frac{\partial u(x,y)}{\partial x} + \sigma(x)\left[\frac{\partial^2 u(x,y)}{\partial x^2} + \frac{\partial^2 u(x,y)}{\partial y^2}\right] = h(x,y),\ (x,y) \in \Omega_j, \tag{4}$$

$$\left.\begin{array}{l} u(x,y_j) = f(x) \\ u_y(x,y_j) = g(x) \end{array}\right\} \text{Cauchy data at the bottom of the } j\text{-th strip}, \tag{5}$$

$$u(0,y) = u_0(y), \tag{6}$$

$$u(\ell_x,y) = u_{\ell_x}(y), \tag{7}$$

where $h(x,y)$, $u_0(y)$ and $u_{\ell_x}(y)$ are all specified functions. *Here, to simplify notation we write $\sigma(x)$ instead of $\sigma^j(x)$, and $\sigma(x) > 0$ is to be determined in each strip*. The term $\sigma'(y)\partial u/\partial y$ disappears from Eq. (4), because in a finite strip of small height

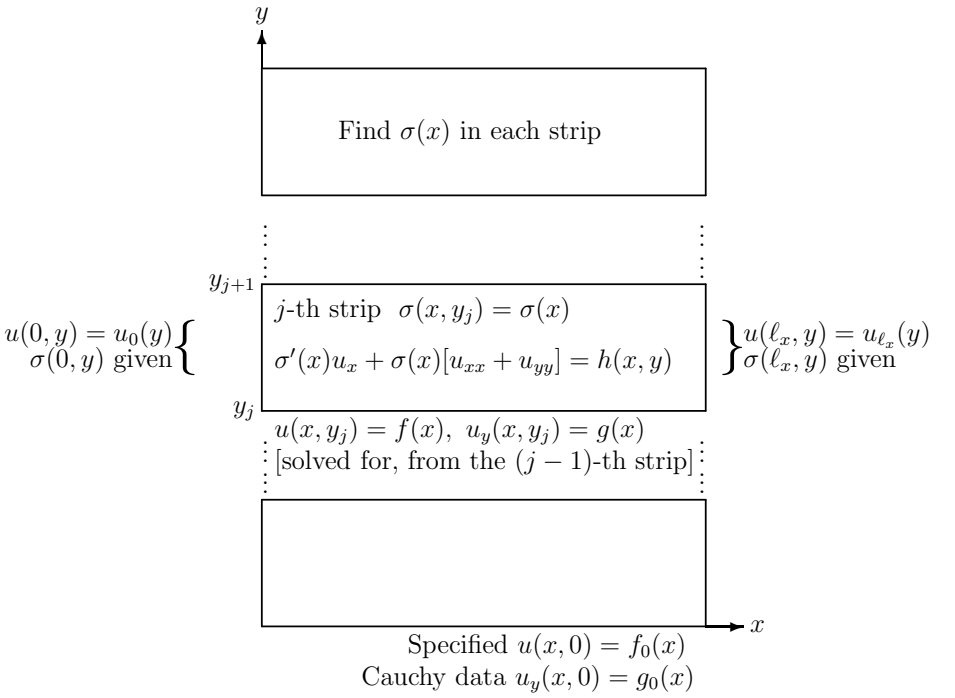

Figure 2: A schematic diagram of the reduced Calderón's inverse problem to identify $\sigma(x)$ in a finite-strip.

$y_{j+1} - y_j$, σ can be approximated by $\sigma(x, y_j)$, which is a function of x alone, and hence, $\sigma'(y) = 0$. In the above, $f(x)$ and $g(x)$ are obtained from the computation performed in the $(j-1)$-th strip. For the first strip, $f(x)$ and $g(x)$ are provided by the Cauchy data, i.e., measurements carried out on the bottom of Ω. In the case when $\sigma(x)$ is given, the above problem is a typical inverse Cauchy problem in each strip with the data on the upper side of the strip being unknown, but the data on the bottom of the strip being over-specified by Eq. (5) [Cauchy data].

Thus, the Calderón inverse problem in a rectangular domain possesses *three-fold simultaneous difficulties: ill-posedness of the inverse Cauchy problem, ill-posedness of the parameter identification, and no information on the impedance function inside the domain being available*.

The finite-strip method described here is somewhat similar to that used by Sylvester (1992), and Somersalo, Cheney, Isaacson and Isaacson (1991) in other situations.

3 The numerical method of lines, to reduce the problem to a system of ODEs

Now, we treat the inverse Cauchy problem and the parameter identification problem in the j-th strip by using the group-preserving scheme, and a Lie-group adaptive method to solve the resulting system of ODEs. Liu (2006) has extended the group preserving scheme (GPS) developed previously by Liu (2001) for ODEs, to solve the boundary value problems (BVPs). In the construction of the Lie-group method for the calculations of BVPs, Liu (2006) has introduced the idea of one-step GPS by utilizing the closure property of the Lie group, and hence, the resulting shooting method has been named the Lie-group shooting method (LGSM). The Lie-group method possesses a great advantage over other numerical methods, due to its group structure, and it is a powerful technique to solve the inverse problem of parameter identification [Liu (2008a, 2008b)].

To simplify the notations, we use y_0 and y_f to denote y_j and y_{j+1}, respectively. First, let $v(x,y) = \partial u(x,y)/\partial y$, and then Eq. (4) can be rewritten as

$$\frac{\partial u(x,y)}{\partial y} = v(x,y), \tag{8}$$

$$\frac{\partial v(x,y)}{\partial y} = \frac{1}{\sigma(x)}\left[h(x,y) - \sigma'(x)\frac{\partial u(x,y)}{\partial x} - \sigma(x)\frac{\partial^2 u(x,y)}{\partial x^2}\right]. \tag{9}$$

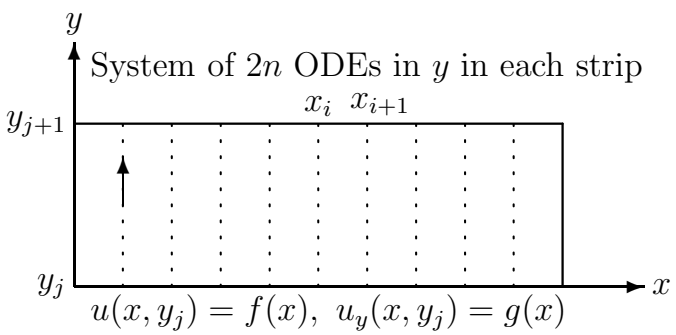

Figure 3: Lie-group shooting method to solve 2n coupled ODEs along these dotted lines.

Second, we use a semi-discretization method[1] of finite-differences to discretize the quantities of $u(x,y)$ and $v(x,y)$ along the x-direction, and thus we can obtain a

[1] While a finite-difference method is used in the x-direction, as an illustration in the present paper, any number of alternate weak-solution methods may be employed in the x-direction in each strip.

system of $2n$-ODEs for u and v, with y as an independent variable [see Fig. 3]:

$$u_i'(y) = v_i(y), \quad [\text{at } x_i,\ i = 1,\ldots,n], \tag{10}$$

$$v_i'(y) = \frac{1}{\sigma_i}\left[h_i(y) - \frac{1}{(\Delta x)^2}\left(\sigma_{i+1}[u_{i+1}(y) - u_i(y)] - \sigma_i[u_i(y) - u_{i-1}(y)]\right)\right],$$
$$[\text{at } x_i,\ i = 1,\ldots,n], \tag{11}$$

where the prime denotes the differential with respect to y, $\Delta x = \ell_x/(n+1)$ is a uniform spatial grid length in the x-direction with n the number of interior grid points in a strip, and $x_i = i\Delta x$ are the discretized coordinates of x, at which $u_i(y) = u(x_i, y)$, $v_i(y) = v(x_i, y)$, $h_i(y) = h(x_i, y)$, and $\sigma_i = \sigma(x_i)$.

When $i = 1$ in Eq. (11), the term $u_0(y)$ appearing there is determined by the boundary condition in Eq. (6). Similarly, when $i = n$, the term $u_{n+1}(y) = u_{\ell_x}(y)$ is determined by the boundary condition in Eq. (7). On the other hand, the term σ_{n+1} is supposed to be measurable at the right-boundary.

The two over-specified boundary conditions on the bottom of the j-th strip are given by

$$u_i(y_j) = f(x_i), \quad i = 1,\ldots,n, \tag{12}$$

$$v_i(y_j) = g(x_i), \quad i = 1,\ldots,n, \tag{13}$$

which are obtained from Eq. (5) by the discretizations at the spatial points x_i. Eqs. (12) and (13) are available through measurements for the first strip, and after that the boundary conditions on the bottom of each other strip are obtained by solving a combination of the inverse Cauchy problem and the parameter identification problem from the previous strip.

Eqs. (10) and (11) constitute a system of $2n$ coupled ODEs involving the discrete values of the unknown function σ_i [at x_i, $i = 1,\ldots,n$ in the j-th strip in the y-direction]; see Fig. 3. We propose to solve these equations through a Lie-group shooting method [Liu (2006)], which is adaptively modified further in the present paper, as described in the following Sections 4-6.

4 A Lie-group formulation

In order to explore the present method of solving the Calderón problem, in a reasonably self-contained fashion, we first briefly sketch the group-preserving scheme (GPS) and the one-step GPS for a general system of ODEs, in this section.

4.1 The group-preserving scheme

We write Eqs. (10) and (11) in a vector form:

$$\mathbf{z}' = \mathbf{f}(y, \mathbf{z}), \tag{14}$$

where

$$\mathbf{z} := \begin{bmatrix} \mathbf{u} \\ \mathbf{v} \end{bmatrix}, \quad \mathbf{f} = \begin{bmatrix} \mathbf{f}_1 \\ \mathbf{f}_2 \end{bmatrix} := \begin{bmatrix} \mathbf{v} \\ \mathbf{f}_2(y, \mathbf{u}) \end{bmatrix}, \tag{15}$$

in which $\mathbf{u} = (u_1, \ldots, u_n)^{\mathrm{t}}$ and $\mathbf{v} = (v_1, \ldots, v_n)^{\mathrm{t}}$ with the superscript $^{\mathrm{t}}$ for the transpose. The components of $\mathbf{f}_2$ represent the right-hand side of Eq. (11).

When both the vector $\mathbf{z}$ and its magnitude $\|\mathbf{z}\| := \sqrt{\mathbf{z}^{\mathrm{t}}\mathbf{z}} = \sqrt{\mathbf{z} \cdot \mathbf{z}}$ are combined into a single augmented vector

$$\mathbf{X} = \begin{bmatrix} \mathbf{z} \\ \|\mathbf{z}\| \end{bmatrix}, \tag{16}$$

Liu (2001) has transformed Eq. (14) into an augmented system:

$$\mathbf{X}' = \mathbf{A}\mathbf{X} := \begin{bmatrix} \mathbf{0}_{2n\times 2n} & \frac{\mathbf{f}(y,\mathbf{z})}{\|\mathbf{z}\|} \\ \frac{\mathbf{f}^{\mathrm{t}}(y,\mathbf{z})}{\|\mathbf{z}\|} & 0 \end{bmatrix} \mathbf{X}, \tag{17}$$

where $\mathbf{A}$ is an element of the Lie algebra $so(2n, 1)$ satisfying

$$\mathbf{A}^{\mathrm{t}}\mathbf{g} + \mathbf{g}\mathbf{A} = \mathbf{0}, \tag{18}$$

and

$$\mathbf{g} = \begin{bmatrix} \mathbf{I}_{2n} & \mathbf{0}_{2n\times 1} \\ \mathbf{0}_{1\times 2n} & -1 \end{bmatrix} \tag{19}$$

is a Minkowski metric. Here, $\mathbf{I}_{2n}$ is the identity matrix.

The augmented variable $\mathbf{X}$ can be viewed as a point in the Minkowski space $\mathbb{M}^{2n+1}$, satisfying the cone condition:

$$\mathbf{X}^{\mathrm{t}}\mathbf{g}\mathbf{X} = \mathbf{z} \cdot \mathbf{z} - \|\mathbf{z}\|^2 = 0. \tag{20}$$

Accordingly, Liu (2001) has developed a group preserving scheme (GPS) to guarantee that each $\mathbf{X}_k$ automatically locates on the cone:

$$\mathbf{X}_{k+1} = \mathbf{G}(k)\mathbf{X}_k, \tag{21}$$

where $\mathbf{X}_k$ denotes the numerical value of $\mathbf{X}$ at the discrete point y_k, and $\mathbf{G}(k) \in SO_o(2n,1)$ satisfies

$$\mathbf{G}^{\mathrm{t}}\mathbf{g}\mathbf{G} = \mathbf{g}, \tag{22}$$

$$\det \mathbf{G} = 1, \tag{23}$$

$$G_0^0 > 0, \tag{24}$$

where G_0^0 is the 00-th component of $\mathbf{G}$.

4.2 One-step Lie-group transformation

Throughout this paper we use the superscripted symbol $\mathbf{z}^0$ to denote the value of $\mathbf{z}$ at $y = y_0$, and $\mathbf{z}^f$ the value of $\mathbf{z}$ at $y = y_f$.

Applying scheme (21) to Eq. (17) with the condition $\mathbf{X}(y_0) = \mathbf{X}^0$ we can compute $\mathbf{X}(y)$ by the GPS. Assuming that the stepsize used in the GPS is $\Delta y = (y_f - y_0)/K$, and starting from an augmented condition $\mathbf{X}^0 = ((\mathbf{z}^0)^{\mathrm{t}}, \|\mathbf{z}^0\|)^{\mathrm{t}} \neq \mathbf{0}$ we will calculate the value of $\mathbf{X}^f = ((\mathbf{z}^f)^{\mathrm{t}}, \|\mathbf{z}^f\|)^{\mathrm{t}}$ at a final $y = y_f$.

By applying Eq. (21) to Eq. (17) step-by-step we can obtain

$$\mathbf{X}^f = \mathbf{G}_K \cdots \mathbf{G}_1 \mathbf{X}^0. \tag{25}$$

Because each $\mathbf{G}_i,\ i = 1, \ldots, K$, is an element of the Lie group $SO_o(2n,1)$, and by the closure property of the Lie group, $\mathbf{G}_K \cdots \mathbf{G}_1$ is also a Lie-group element denoted by $\mathbf{G}$. Hence, from Eq. (25) it follows that

$$\mathbf{X}^f = \mathbf{G}\mathbf{X}^0, \tag{26}$$

which is a one-step Lie-group transformation from $\mathbf{X}^0$ to $\mathbf{X}^f$ [Liu (2009b); Liu (2010a)].

The above property is crucial for our development of the Lie-group method. It should be stressed that the one-step Lie-group transformation property is usually not shared by other numerical methods, because those methods do not belong to the Lie-group schemes.

The remaining problem is how to calculate $\mathbf{G}$. While an exact solution of $\mathbf{G}$ is not available, we can calculate $\mathbf{G}$ through the numerical algorithm of a generalized mid-point rule, which is obtained from an exponential mapping of $\mathbf{A}$ by taking the values of the argument variables of $\mathbf{A}$ at a generalized mid-point. The Lie-group element generated from such an $\mathbf{A} \in so(2n,1)$ by an exponential mapping is

$$\mathbf{G}(r) = \begin{bmatrix} \mathbf{I}_{2n} + \frac{a-1}{\|\hat{\mathbf{f}}\|^2}\hat{\mathbf{f}}\hat{\mathbf{f}}^{\mathrm{t}} & \frac{b\hat{\mathbf{f}}}{\|\hat{\mathbf{f}}\|} \\ \frac{b\hat{\mathbf{f}}^{\mathrm{t}}}{\|\hat{\mathbf{f}}\|} & a \end{bmatrix}, \tag{27}$$

where

$$\hat{\mathbf{z}} = r\mathbf{z}^0 + (1-r)\mathbf{z}^f, \tag{28}$$

$$\hat{\mathbf{f}} = \mathbf{f}(\hat{y}, \hat{\mathbf{z}}), \tag{29}$$

$$a = \cosh\left(\frac{(y_f - y_0)\|\hat{\mathbf{f}}\|}{\|\hat{\mathbf{z}}\|}\right), \quad b = \sinh\left(\frac{(y_f - y_0)\|\hat{\mathbf{f}}\|}{\|\hat{\mathbf{z}}\|}\right). \tag{30}$$

Here, we have derived a single-parameter Lie-group element $\mathbf{G}(r)$ in terms of $r \in [0,1]$, and $\hat{y} = ry_0 + (1-r)y_f$.

4.3 A two-point Lie-group equation

Upon defining

$$\mathbf{F} := \frac{\hat{\mathbf{f}}}{\|\hat{\mathbf{z}}\|}, \tag{31}$$

Eqs. (27) and (30) can be expressed as

$$\mathbf{G} = \begin{bmatrix} \mathbf{I}_{2n} + \frac{a-1}{\|\mathbf{F}\|^2}\mathbf{F}\mathbf{F}^{\mathrm{t}} & \frac{b\mathbf{F}}{\|\mathbf{F}\|} \\ \frac{b\mathbf{F}^{\mathrm{t}}}{\|\mathbf{F}\|} & a \end{bmatrix}, \tag{32}$$

$$a = \cosh[(y_f - y_0)\|\mathbf{F}\|], \quad b = \sinh[(y_f - y_0)\|\mathbf{F}\|]. \tag{33}$$

From Eqs. (16), (26) and (32) it follows that

$$\mathbf{z}^f = \mathbf{z}^0 + \eta\mathbf{F}, \tag{34}$$

$$\|\mathbf{z}^f\| = a\|\mathbf{z}^0\| + b\frac{\mathbf{F}\cdot\mathbf{z}^0}{\|\mathbf{F}\|}, \tag{35}$$

where

$$\eta := \frac{(a-1)\mathbf{F}\cdot\mathbf{z}^0 + b\|\mathbf{z}^0\|\|\mathbf{F}\|}{\|\mathbf{F}\|^2}. \tag{36}$$

Eq. (34) is written as

$$\mathbf{F} = \frac{1}{\eta}(\mathbf{z}^f - \mathbf{z}^0). \tag{37}$$

Substituting $\mathbf{F}$ into Eq. (35), and dividing both the sides by $\|\mathbf{z}^0\|$, we can obtain

$$\frac{\|\mathbf{z}^f\|}{\|\mathbf{z}^0\|} = a + b\frac{(\mathbf{z}^f - \mathbf{z}^0)\cdot\mathbf{z}^0}{\|\mathbf{z}^f - \mathbf{z}^0\|\|\mathbf{z}^0\|}, \tag{38}$$

where, after inserting Eq. (37) for $\mathbf{F}$ into Eq. (33), a and b are written as

$$a = \cosh\left(\frac{(y_f - y_0)\|\mathbf{z}^f - \mathbf{z}^0\|}{\eta}\right), \quad b = \sinh\left(\frac{(y_f - y_0)\|\mathbf{z}^f - \mathbf{z}^0\|}{\eta}\right). \tag{39}$$

Let

$$\cos\theta := \frac{(\mathbf{z}^f - \mathbf{z}^0)\cdot \mathbf{z}^0}{\|\mathbf{z}^f - \mathbf{z}^0\|\|\mathbf{z}^0\|}, \tag{40}$$

$$S := (y_f - y_0)\|\mathbf{z}^f - \mathbf{z}^0\|, \tag{41}$$

and from Eqs. (38) and (39) it follows that

$$\frac{\|\mathbf{z}^f\|}{\|\mathbf{z}^0\|} = \cosh\left(\frac{S}{\eta}\right) + \cos\theta \sinh\left(\frac{S}{\eta}\right). \tag{42}$$

Upon defining

$$Z := \exp\left(\frac{S}{\eta}\right), \tag{43}$$

we can derive [Liu (2008b, 2010a, 2010b)]

$$Z = \frac{(\cos\theta - 1)\|\mathbf{z}^0\|}{\cos\theta\|\mathbf{z}^0\| + \|\mathbf{z}^f - \mathbf{z}^0\| - \|\mathbf{z}^f\|}. \tag{44}$$

From Eqs. (43) and (41) it follows that

$$\eta = \frac{(y_f - y_0)\|\mathbf{z}^f - \mathbf{z}^0\|}{\ln Z}. \tag{45}$$

Therefore, we arrive to an important result that between any two points $(\mathbf{z}^0, \|\mathbf{z}^0\|)$ and $(\mathbf{z}^f, \|\mathbf{z}^f\|)$ on the cone, there exists a Lie-group element $\mathbf{G} \in SO_o(2n,1)$ mapping $(\mathbf{z}^0, \|\mathbf{z}^0\|)$ onto $(\mathbf{z}^f, \|\mathbf{z}^f\|)$, which is given by

$$\begin{bmatrix} \mathbf{z}^f \\ \|\mathbf{z}^f\| \end{bmatrix} = \mathbf{G}(y_0, y_f) \begin{bmatrix} \mathbf{z}^0 \\ \|\mathbf{z}^0\| \end{bmatrix}. \tag{46}$$

$\mathbf{G}(y_0, y_f)$ is uniquely determined by $\mathbf{z}^0$ and $\mathbf{z}^f$ through the following equations:

$$\mathbf{G}(y_0, y_f) = \begin{bmatrix} \mathbf{I}_{2n} + \frac{a-1}{\|\mathbf{F}\|^2}\mathbf{F}\mathbf{F}^{\mathrm{t}} & \frac{b\mathbf{F}}{\|\mathbf{F}\|} \\ \frac{b\mathbf{F}^{\mathrm{t}}}{\|\mathbf{F}\|} & a \end{bmatrix}, \tag{47}$$

$$a = \cosh[(y_f - y_0)\|\mathbf{F}\|], \quad b = \sinh[(y_f - y_0)\|\mathbf{F}\|], \tag{48}$$

$$\mathbf{F} = \frac{1}{\eta}(\mathbf{z}^f - \mathbf{z}^0) = \frac{\ln Z}{y_f - y_0}\frac{\mathbf{z}^f - \mathbf{z}^0}{\|\mathbf{z}^f - \mathbf{z}^0\|}. \tag{49}$$

We should emphasize that the above $\mathbf{G}(y_0, y_f)$ is different from the $\mathbf{G}(r)$ in Eq. (27). In order to feature its property as being a Lie-group mapping between the quantities spanned a whole interval of $[y_0, y_f]$ we write it to be $\mathbf{G}(y_0, y_f)$, which is independent on $\mathbf{f}$ and r. Conversely, $\mathbf{G}(r)$ is a function of r and $\mathbf{f}$. However, these two Lie-group elements $\mathbf{G}(r)$ and $\mathbf{G}(y_0, y_f)$ are necessary in our development of the Lie-group method, which is coined as the following *two-point Lie-group equation*:

$$\mathbf{z}^f = \mathbf{z}^0 + \frac{\eta}{\|\hat{\mathbf{z}}\|}\hat{\mathbf{f}}. \tag{50}$$

By Eq. (45) a more symmetric form can be obtained:

$$\frac{\mathbf{z}^f - \mathbf{z}^0}{\|\mathbf{z}^f - \mathbf{z}^0\|} = \frac{y_f - y_0}{\ln Z}\frac{\hat{\mathbf{f}}}{\|\hat{\mathbf{z}}\|}. \tag{51}$$

In the next section for the inverse problem of recovering an unknown coefficient, we employ the above equation to derive a system of non-linear algebriac equations to solve for $\sigma(x)$.

5 The Lie-group method

From Eqs. (10)-(13) it follows that

$$\mathbf{u}' = \mathbf{v}, \tag{52}$$
$$\mathbf{v}' = \mathbf{f}_2(y, \mathbf{u}), \tag{53}$$
$$\mathbf{u}(y_0) = \mathbf{u}^0, \ \ \mathbf{u}(y_f) = \mathbf{u}^f, \tag{54}$$
$$\mathbf{v}(y_0) = \mathbf{v}^0, \ \ \mathbf{v}(y_f) = \mathbf{v}^f, \tag{55}$$

where $\mathbf{u}^0$ and $\mathbf{v}^0$ are specified as in Eqs. (12) and (13).

By using Eq. (15) for $\mathbf{z}$ we have

$$\mathbf{z}^0 = \begin{bmatrix} \mathbf{u}^0 \\ \mathbf{v}^0 \end{bmatrix}, \ \ \mathbf{z}^f = \begin{bmatrix} \mathbf{u}^f \\ \mathbf{v}^f \end{bmatrix}, \tag{56}$$

and by Eq. (50) we can derive

$$\mathbf{u}^f = \mathbf{u}^0 + \frac{\eta}{\|\hat{\mathbf{z}}\|}\hat{\mathbf{v}}, \tag{57}$$
$$\mathbf{v}^f = \mathbf{v}^0 + \frac{\eta}{\|\hat{\mathbf{z}}\|}\hat{\mathbf{f}}_2, \tag{58}$$

where

$$\begin{aligned}\|\hat{\mathbf{z}}\| &= \sqrt{\|\hat{\mathbf{u}}\|^2+\|\hat{\mathbf{v}}\|^2} \\ &= \sqrt{\|r\mathbf{u}^0+(1-r)\mathbf{u}^f\|^2+\|r\mathbf{v}^0+(1-r)\mathbf{v}^f\|^2},\end{aligned} \tag{59}$$

$$\hat{\mathbf{f}}_2 = \begin{bmatrix} \frac{\hat{h}_1}{\sigma_1}-\frac{1}{\sigma_1(\Delta x)^2}[\sigma_2(\hat{u}_2-\hat{u}_1)-\sigma_1(\hat{u}_1-\hat{u}_0)] \\ \frac{\hat{h}_2}{\sigma_2}-\frac{1}{\sigma_2(\Delta x)^2}[\sigma_3(\hat{u}_3-\hat{u}_2)-\sigma_2(\hat{u}_2-\hat{u}_1)] \\ \vdots \\ \frac{\hat{h}_{n-1}}{\sigma_{n-1}}-\frac{1}{\sigma_{n-1}(\Delta x)^2}[\sigma_n(\hat{u}_n-\hat{u}_{n-1})-\sigma_{n-1}(\hat{u}_{n-1}-\hat{u}_{n-2})] \\ \frac{\hat{h}_n}{\sigma_n}-\frac{1}{\sigma_n(\Delta x)^2}[\sigma_{n+1}(\hat{u}_{n+1}-\hat{u}_n)-\sigma_n(\hat{u}_n-\hat{u}_{n-1})] \end{bmatrix}, \tag{60}$$

where $\hat{u}_i = ru_i^0+(1-r)u_i^f$, $\hat{h}_i = h_i(\hat{y})$, and $\hat{u}_0 = u_0(\hat{y})$ and $\hat{u}_{n+1} = u_{\ell_x}(\hat{y})$.
From Eqs. (58) and (60) we can derive a formula to calculate σ_i:

$$\sigma_i = \frac{1}{\frac{\hat{u}_i-\hat{u}_{i-1}}{(\Delta x)^2}-\frac{\|\hat{\mathbf{z}}\|}{\eta}(v_i^f-v_i^0)}\left[\frac{\hat{u}_{i+1}-\hat{u}_i}{(\Delta x)^2}\sigma_{i+1}-\hat{h}_i\right]. \tag{61}$$

Eq. (61) can be used sequentially to find σ_i, $i=n,\ldots,1$, if we know σ_{n+1} a priori. Here, σ_{n+1} is the right-boundary value of σ in the j-th strip, which is supposed to be measurable. Because η is a nonlinear function of u_i^f and v_i^f, Eq. (61) provides us a mathematical tool to calculate σ_i.

6 An iterative Lie-group method to compute $\sigma(x)$ in the Calderón inverse problem

Now, the numerical procedures for estimating σ_i are described as follows. First, we assume a "guess" value for σ_i, for example, a linear variation $\sigma_i = \sigma(0)+x_i/\ell_x[\sigma(\ell_x)-\sigma(0)]$. Here, $\sigma(0)$ and $\sigma(\ell_x)$ are the given boundary values of σ in the j-th strip. Substituting σ_i into Eqs. (10) and (11) we can apply the GPS to integrate them from $y=y_0$ to $y=y_f$. Then, we can obtain u_i^f and v_i^f, and inserting them into Eq. (61) we can calculate a new σ_i, which is then compared with the old σ_i. If the difference of these two sets of σ_i is smaller than a given criterion, then we stop the iteration, and the final σ_i is obtained. The numerical processes are summarized as follows:

Step 1: Give an initial "guess" value for σ_i.
Step 2: For $k = 1, 2 \ldots$ we repeat the following calculations. Calculate u_i^f and v_i^f by using the GPS to integrate Eqs. (10) and (11) from $y = y_0$ to $y = y_f$.
Step 3: Insert the above calculated u_i^f and v_i^f, denoted respectively by $u_i^f(k)$ and $v_i^f(k)$, together with u_i^0 and v_i^0 given by Eqs. (12) and (13) into

$$\sigma_i(k) = \frac{1}{\frac{\hat{u}_i(k)-\hat{u}_{i-1}(k)}{(\Delta x)^2} - \frac{\|\hat{\mathbf{z}}(k)\|}{\eta(k)}[v_i^f(k) - v_i^0]} \left[\frac{\hat{u}_{i+1}(k) - \hat{u}_i(k)}{(\Delta x)^2} \sigma_{i+1}(k) - \hat{h}_i \right], \tag{62}$$

where $\eta(k)$ and $\|\hat{\mathbf{z}}(k)\|$ are calculated from Eqs. (45) and (59) by inserting $u_i^f(k)$, $v_i^f(k)$, u_i^0 and v_i^0. If $\sigma_i(k)$ converges according to a given convergence criterion:

$$C_k =: \sqrt{\sum_{i=1}^{n} [\sigma_i(k+1) - \sigma_i(k)]^2} < \varepsilon, \tag{63}$$

then stop; otherwise, go to **Step 2**. C_k measures the convergence speed.

Basically, in the present method we have derived Eq. (62) by supposing a fictitious target $u_i^f(k)$ and $v_i^f(k)$ at y_f. We can repeatedly use the y-direction GPS integrator on Eqs. (10) and (11), to obtain the new final data, which are not obtained through the measurements, and then we can adjust σ_i by Eq. (62). Because we have used the iteration process as a combination of the GPS and the two-point Lie-group equation with a fictitious target, the present algorithm is quite different from other algorithms. In order to differentiate the present method from the earlier ones, we may call it an iterative and adaptive Lie-group method, wherein the adaptations are performed by the governing equations themselves.

Although there is a number of numerical algorithms to treat the inverse Cauchy problem, we found that the GPS presented in Section 4.1 is the simplest one, which is a stable scheme for the inverse Cauchy problem in a small strip.

In summary, the methodology used in this paper is the use of a simple and stable GPS method to treat the inverse Cauchy problem, and then using the iterative Lie-group method to find σ_i in each strip. These procedures are repeated in the whole domain by solving the above problems strip-by-strip. The philosophy of the solution methodology of the iterative and adaptive Lie-group method is that the *local differential equation* (11) and the *global algebraic equation* (61) must self-adapt to a situation that they are compatible, such that σ_i can be computed from them through a self-adaptive process.

7 Numerical verifications

From the above discussions one can appreciate that the present method, which represents a combination of the finite strip method, the GPS and the iterative and adaptive Lie-group method, quite simple and straightforward, is easy to implement numerically and the computational cost is very low. In order to assess the performance of the present method, we test the following numerical examples of Calderón inverse problems.

7.1 Example 1

This numerical example is a simplified one of identifying a function of $\sigma(x)$ in a finite strip, which is designed to validate and test the presently proposed method for the inverse Cauchy problem and the parameter identification problem. We first consider the model problem when $u(x,y)$, $\sigma(x)$, and $h(x,y)$ are taken to be

$$u(x,y) = (x-3)^2 e^{-y}, \tag{64}$$

$$\sigma(x) = (x-3)^2, \tag{65}$$

$$h(x,y) = 6(x-3)^2 e^{-y} + (x-3)^4 e^{-y}. \tag{66}$$

From Eq. (64), we can derive the following boundary conditions:

$$u(0,y) = 9e^{-y}, \;\; u(1,y) = 4e^{-y}, \tag{67}$$

and the over-specified Cauchy boundary conditions on the bottom of the strip:

$$u(x,0) = (x-3)^2, \;\; u_y(x,0) = -(x-3)^2. \tag{68}$$

We use the boundary conditions (67) and (68) and $h(x,y)$ in Eq. (66) to solve the Calderón's inverse problem *of finding* $\sigma(x)$, and compare it to the presumed exact solution $\sigma(x) = (x-3)^2$.

We first directly apply the GPS to integrate Eqs. (10) and (11), taking $\sigma(x)$ to be as given in Eq. (65). We use the GPS to compute the data on the upper side of the strip with a depth $y_f = 0.05$, given the boundary data as in Eqs. (67) and (68). In Figs. 4(a) and 4(b) we show the numerical errors by comparing the numerically computed results for u at the top of the strip, with the exact solutions for u as derived from Eq. (64) by inserting $y = 0.05$. In this calculation by the GPS, we use $\Delta x = 1/40$, and $\Delta y = 0.05/100$, where Δy is a stepsize used in the integration of Eqs. (10) and (11) by the GPS. It can be seen that the numerical error of the Dirichlet data at the top of the strip is quite small, in the order of 10^{-5}, while the

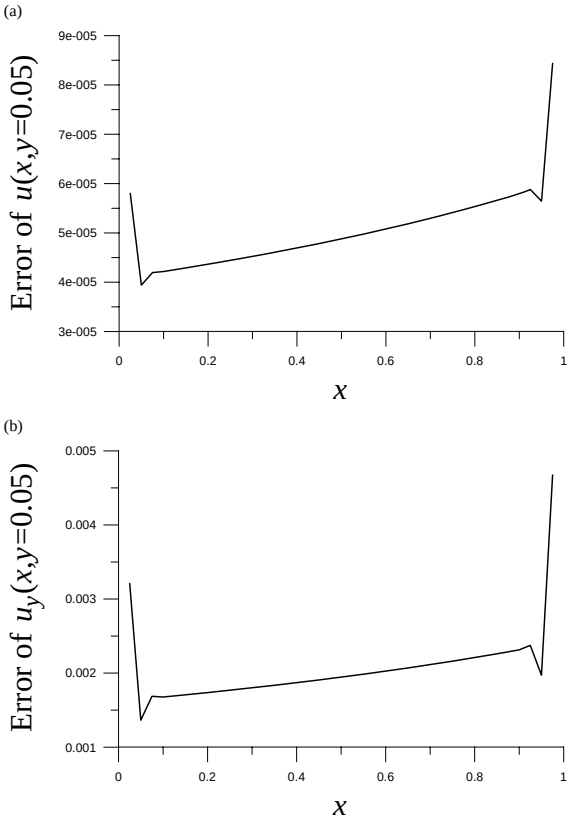

Figure 4: For example 1 of the inverse Cauchy problem, the numerical errors obtained by the GPS are shown for (a) the Dirichlet data, and (b) the Neumann data.

numerical error of the Neumann data at the top of the strip is small in the order of 10^{-3}.

Now, we use the above example again *to identify the parameter* $\sigma(x)$ in a small strip with $y_f = 0.03$, given $h(x,y)$ as in Eq. (66) and the boundary-data on the strip as in Eqs. (67) and (68). We apply the iterative and adaptive Lie-group method of this paper to this problem, where we fix $r = 0$ in Eq. (62), $\Delta x = 1/30$, and $\Delta y = 0.03/100$. Under an exit criterion with $\varepsilon = 10^{-3}$, the process is convergent within 212 iterations. In Fig. 5(a) we show the rate of convergence, and in Fig. 5(b) we compare the numerically recovered σ_i with the postulated exact one of Eq. (65). The numerically recovered σ_i is almost coincident with the exact one.

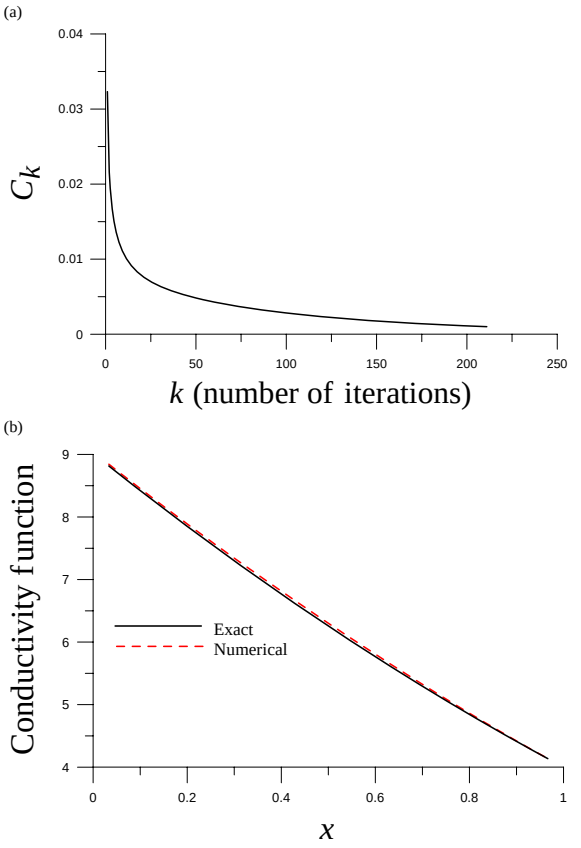

Figure 5: For example 1: (a) the rate of convergence, and (b) numerical and exact solutions are shown.

7.2 Example 2

We now consider the problem of recovering the conductivity function $\sigma(x,y)$ in the entire domain. We consider the case when the exact solution $u(x,y)$ $[0 \le x \le \ell_x,\ 0 \le y \le \ell_y]$ and when $\sigma(x,y)$ are taken to be

$$u(x,y) = (x-3)^2 e^{-y}, \tag{69}$$

$$\sigma(x,y) = (x-3)^2 + y^2, \ \ (x,y) \in (0,1) \times (0,1). \tag{70}$$

Hence, we have

$$h(x,y) = (6-2y)(x-3)^2 e^{-y} + (x-3)^4 e^{-y}. \tag{71}$$

The conditions on the boundary of Ω, corresponding to the ones schematically shown in Fig. 1 are taken from Eqs. (67) and (68).

We apply the numerical method of iterative and adaptive Lie-group method in Section 6, solve for $u(x,y)$ and $\sigma(x,y)$, given $h(x,y)$ as in Eq, (71), and the boundary conditions are as in Eqs. (67) and (68), and $\sigma(0,y) = 9+y^2$ and $\sigma(1,y) = 4+y^2$. The domain is divided into 40 strips with each strip having a depth $\delta y = 0.025$. The convergence criterion ε is fixed to be $\varepsilon = 10^{-4}$. In addition we take $\Delta x = 1/40$ and $\Delta y = 0.025/20$, where Δy is the stepsize used in the integration by the GPS. In Fig. 6 we compare the exact and numerically recovered conductivity functions, which can be seen to be close. We show the relative errors of the recovery of the above $\sigma(x,y)$ in Fig. 7. The relative error is defined as the absolute value of the difference between numerical solution and exact solution, divided by the value of exact solution. The results are accurate with the maximal relative error being smaller than 0.2. It can be seen that the accuracy for the recovery of $\sigma(x,y)$ is acceptable for the most of the domain (x,y) in the plane of $0 \le x,y \le 1$, except very near the corner $(x,y) = (1,1)$.

7.3 Example 3

In this example we consider a hypothetical exact solution

$$u(x,y) = \exp(2x+2y), \tag{72}$$

$$\sigma(x,y) = \exp(-x-3y), \quad (x,y) \in (0,1) \times (0,2), \tag{73}$$

which leads to $h(x,y) = 0$.

We now consider the inverse Calderón problem of finding $u(x,y)$ and $\sigma(x,y)$, given only the boundary conditions on u and σ as shown in Fig. 1, and derived from Eqs. (72) and (73). We apply the iterative and adaptive Lie-group method to this example. The domain is divided into 40 strips with each strip having a depth $\delta y = 0.05$. We let the convergence criterion ε be quite large, such that there is only one iteration in **Step 3**. We take $\Delta x = 1/100$ and $\Delta y = 0.05/50$, where Δy is the stepsize used in the integration of Eqs. (10) and (11) by the GPS. The exact and numerically recovered conductivity functions are compared in Fig. 8, and can be seen to be rather close to each other. We show the errors of the recovery of the above $\sigma(x,y)$ in Fig. 9. In Fig. 9(a) the absolute errors are projected onto the plane along the y-axis, while in Fig. 9(b) the abolute errors are projected onto the plane along the x-axis. The results are rather accurate with the maximal absolute error being smaller than 7.8×10^{-2}. Starting from the 15-th strip on, the absolute error is smaller than 0.01 and gradually tends to 2.24×10^{-4}.

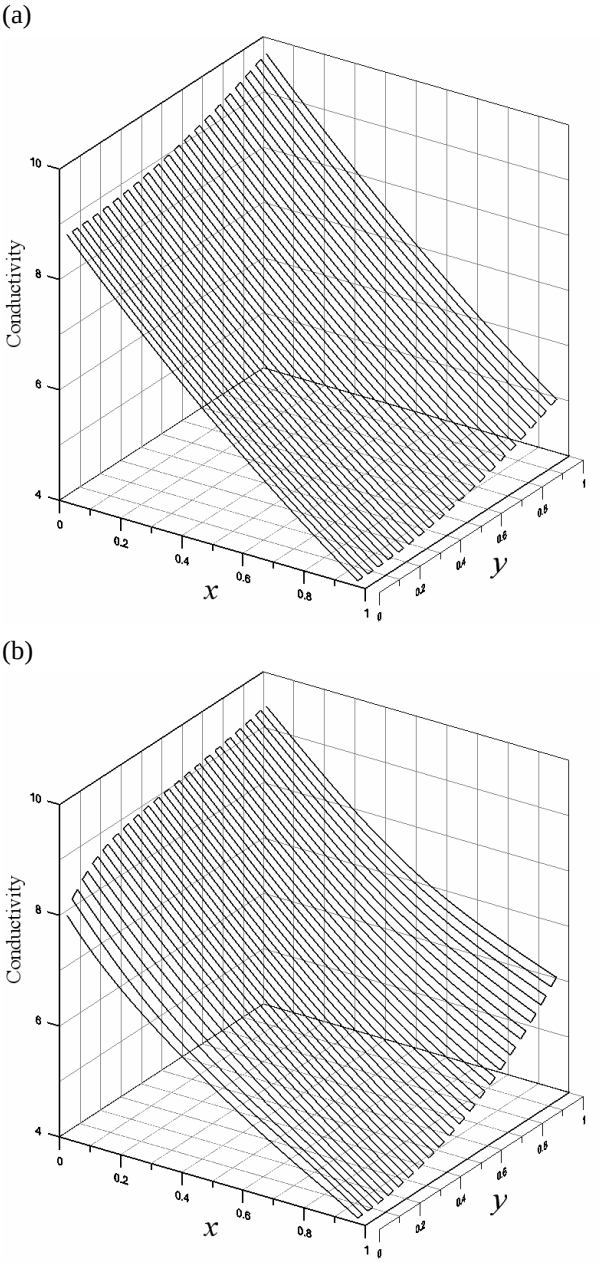

Figure 6: For example 2: (a) exact conductivity function, and (b) numerically recovered conductivity function are compared.

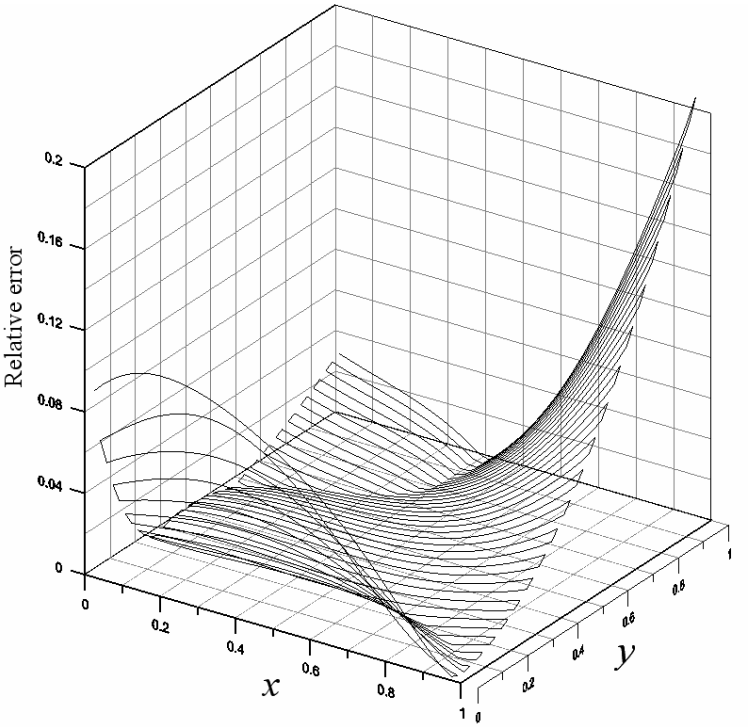

Figure 7: For example 2, the relative errors over the plane of (x,y) are shown.

7.4 Example 4

Next, we test a more difficult problem, with the hypothetical exact solution for $u(x,y)$ as in Eq. (72), and a hypothetical $\sigma(x,y)$ assumed as

$$\sigma(x,y) = 10 + \exp\left[-\frac{(x-0.5)^2}{0.05}\right] \exp\left[-\frac{(y-0.5)^2}{0.05}\right], \quad (x,y) \in (0,1)\times(0,1). \quad (74)$$

Hence, $h(x,y)$ can be calculated as:

$$h(x,y) = \frac{\partial \sigma(x,y)}{\partial x}\frac{\partial u(x,y)}{\partial x} + \frac{\partial \sigma(x,y)}{\partial y}\frac{\partial u(x,y)}{\partial y} + \sigma(x,y)\left[\frac{\partial^2 u(x,y)}{\partial x^2} + \frac{\partial^2 u(x,y)}{\partial y^2}\right]. \quad (75)$$

The explicit expression for the right-hand side of Eq. (75) is quite lengthy, and we do not write it here. Over the plane (x,y), the profile of $\sigma(x,y)$ described by Eq. (74) is a steep hump concentrated at the point $(x,y) = (0.5,0.5)$ with a base

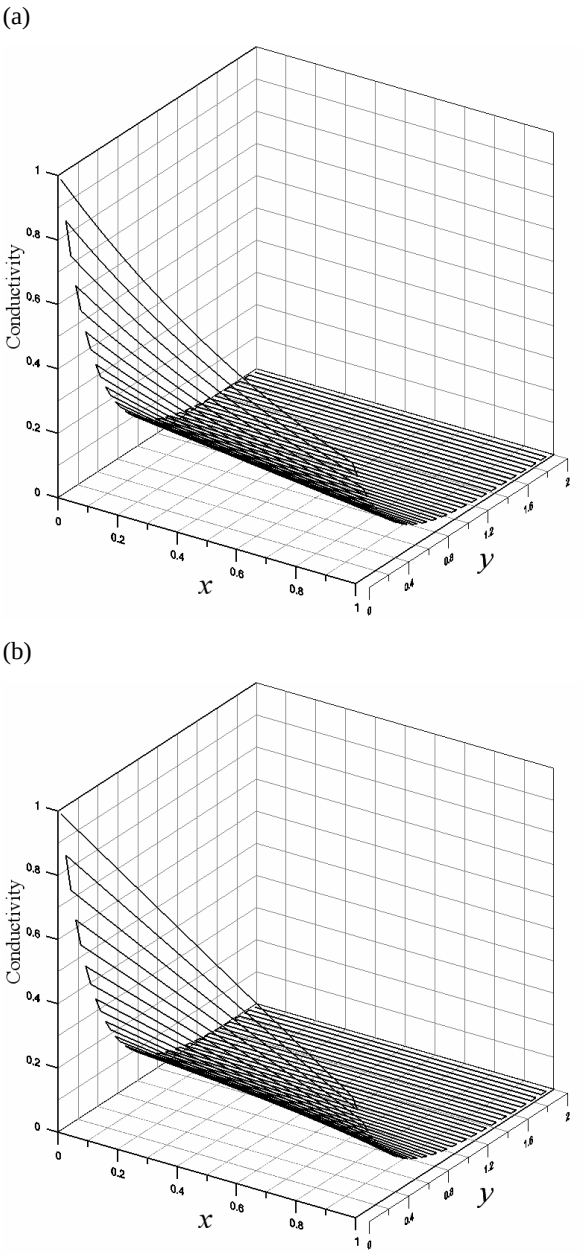

Figure 8: For example 3: (a) exact conductivity function, and (b) numerically recovered conductivity function are compared

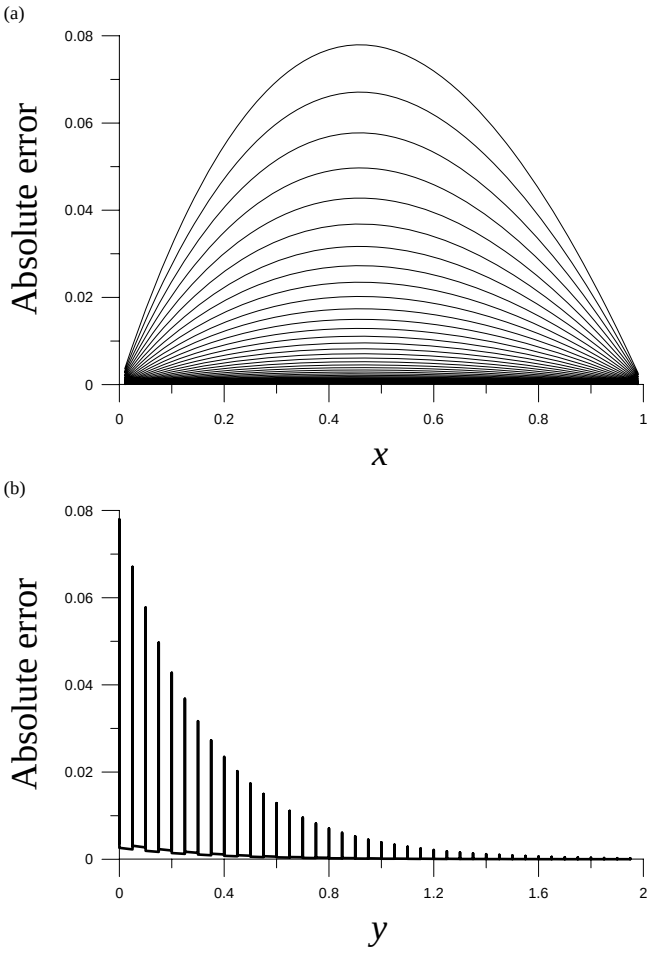

Figure 9: For example 3: (a) the absolute errors by a projection along y-axis, and (b) the absolute errors by a projection along x-axis are shown

value of $\sigma = 10$. Outside the hump, the values of σ are decaying fast to the base value $\sigma = 10$.

We then consider the inverse problem of finding $\sigma(x,y)$ along with $u(x,y)$ for the problem in a unit square $[0 \leq x,y \leq 1]$, when $h(x,y)$ is given as in Eq. (75) and the boundary conditions on σ and u, corresponding to Fig. 1, are derived from Eqs. (74) and (72), respectively. The domain is divided into 50 strips with each strip having a depth $\delta y = 0.02$. We let the convergence criterion ε to be quite large, such that there is only one iteration in **Step 3**. In addition we take $\Delta x = 1/50$ and

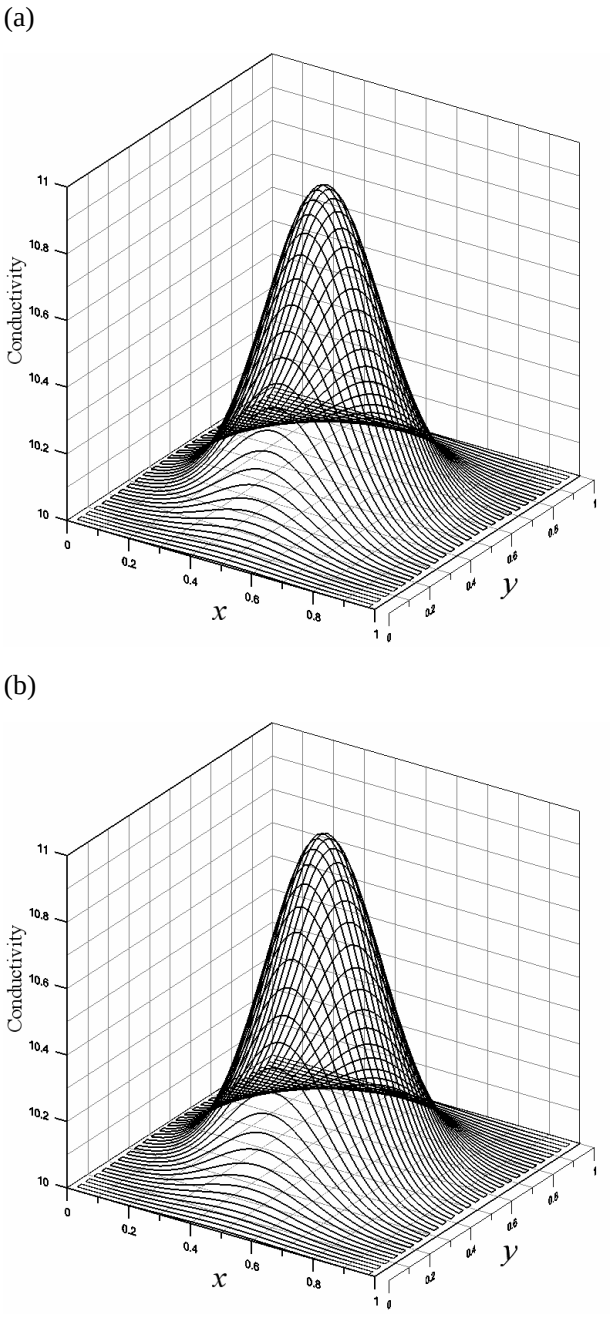

Figure 10: For example 4: (a) exact conductivity function, and (b) numerically recovered conductivity function are compared.

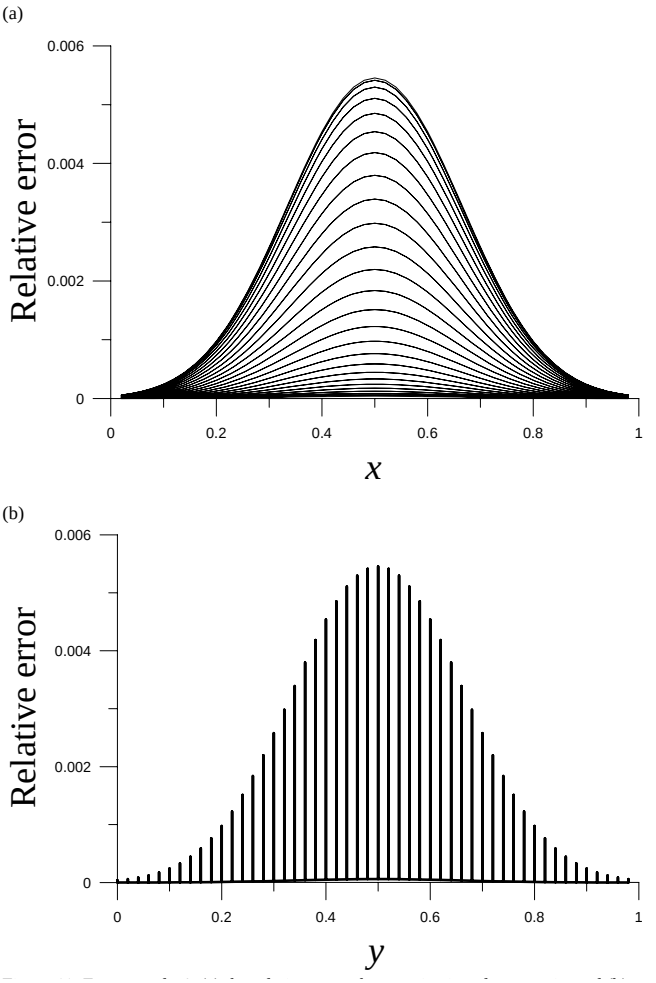

Figure 11: For example 4: (a) the relative errors by a projection along y-axis, and (b) the relative errors by a projection along x-axis are shown.

$\Delta y = 0.02/20$, where Δy is the stepsize used in the integration of the GPS. The exact and numerically recovered conductivity functions are coincident very good as shown in Fig. 10. We show the errors of the recovery of the above $\sigma(x,y)$ in Fig. 11. In Fig. 11(a) the relative errors are projected onto the plane along the y-axis, while in Fig. 11(b) the relative errors are projected onto the plane along the x-axis. The results are quite accurate with the maximal relative error being smaller than 0.006.

8 Conclusions

A finite-strip technique was employed here to transform the inverse Calderón problem in a rectangle, into many inverse Cauchy problems and parameter identification problems within the small strips lying along the x-direction, and of a small finite height in the y-direction. The group-preserving scheme and an iterative and adaptive Lie-group method were then developed for solving the inverse Cauchy problem and the inverse estimation of spatially-dependent conductivity function, in each two-dimensional strip. Specially, we have considered the inverse Calderón problem with over-specified boundary data on the bottom of a rectangle only. Eq. (61) is a critical equation, which plays an important role to adjust the parameter $\sigma(x_i)$ in a strip, through iterations. The unknown conductivity function can be solved explicitly in a closed-form sequential formula, which can generate the correct conductivity coefficients. The advantages of the present method are that no a priori information about the functional form of conductivity function is necessary, and no extra measurement of data inside the domain is required. Indeed, we have successfully solved a quite difficult problem of the Calderón type, as a combination of the inverse Cauchy problem and the parameter identification problem of $\sigma(x,y)$ defined in each finite strip, without being given the data inside the domain. The accuracy and efficiency of the present algorithm are confirmed by comparing the estimated results with exact solutions in diverse situations. The methods presented in the present paper appear quite promising to solve the inverse Calderón problem in domains of arbitrary shape, which are of significiant importance in engineering.

Acknowledgement: Taiwan's National Science Council projects NSC-97-2221-E-002-274-MY3 and NSC-99-2221-E-002-074-MY3 granted to the first author is highly appreciated.

References

Adler, A.; Guardo, R. (1994): A neural network image reconstruction technique for electrical impedance tomography. *IEEE Trans. Med. Imag.*, vol. 13, pp. 594-600.

Borcea, L. (2002): Electrical impedance tomography. *Inverse Problems*, vol. 18, pp. R99-R136.

Borcea, L.; Gray, G. A.; Zhang, Y. (2003): Variationally constrained numerical solution of electrical impedance tomography. *Inverse Problems*, vol. 19, pp. 1159-1184.

Brown, R. M.; Uhlmann, G. A. (1997): Uniqueness in the inverse conductivity problem for non-smooth conductivities in two dimensions. *Comm. Part. Diff. Eq.*, vol. 22, pp. 1009-1027.

Calderón, A. P. (1980): On an inverse boundary value problem, in Seminar on Numerical Analysis and its Application to Continuum Physics, Rio de Janeiro, Brazil: Soc. Brasileira de Mathematica, 1980, pp. 65-73.

Calderón, A. P. (2006): On an inverse boundary value problem. *Comp. Appl. Math.*, vol. 25, pp. 133-138.

Francini, E. (2000): Recoverning a complex coefficient in a planar domain from the Dirichlet-to-Neumann map. *Inverse Problems*, vol. 16, pp. 107-119.

Kaup, P. G.; Santosa, F.; Vogelius, M. (1996): Method for imaging corrosion damage in thin plates from electrostatic data. *Inverse Problems*, vol. 12, pp. 279-293.

Knowles, I. (1998): A variational algorithm for electrical impedance tomography. *Inverse Problems*, vol. 14, pp. 1513-1526.

Kohn, R. V.; McKenney, A. (1990): Numerical implementation of a variational method for electrical impedance tomography. *Inverse Problems*, vol. 6, pp. 389-414.

Levy, S.; Adam, D.; Bresler, Y. (2002): Electromagnetic impedance tomography (EMIT): a new method for impedance imaging. *IEEE Trans. Med. Imag.*, vol. 21, pp. 676-687.

Liu, C.-S. (2001): Cone of non-linear dynamical system and group preserving schemes. *Int. J. Non-Linear Mech.*, vol. 36, pp. 1047-1068.

Liu, C.-S. (2006): The Lie-group shooting method for nonlinear two-point boundary value problems exhibiting multiple solutions. *CMES: Computer Modeling in Engineering & Sciences*, vol. 13, pp. 149-163.

Liu, C.-S. (2008a): An LGSM to identify nonhomogeneous heat conductivity functions by an extra measurement of temperature. *Int. J. Heat Mass Transfer*, vol. 51, pp. 2603-2613.

Liu, C.-S. (2008b): An LGEM to identify time-dependent heat conductivity function by an extra measurement of temperature gradient. *CMC: Computers, Materials & Continua*, vol. 7, pp. 81-95.

Liu, C.-S. (2009a): Solving the inverse problems of Laplace equation to determine the Robin coefficient/cracks' position inside a disk. *CMES: Computer Modeling in Engineering & Sciences*, vol. 40, pp. 1-28.

Liu, C.-S. (2009b): A two-stage LGSM to identify time-dependent heat source through an internal measurement of temperature. *Int. J. Heat Mass Transfer*, vol.

52, pp. 1635-1642.

Liu, C.-S. (2010a): A two-stage Lie-group shooting method (TSLGSM) to identify time-dependent thermal diffusivity. *Int. J. Heat Mass Transfer*, vol. 53, pp. 4876-4884.

Liu, C.-S. (2010b): A highly accurate LGSM for severely ill-posed BHCP under a large noise on the final time data. *Int. J. Heat Mass Transfer*, vol. 53, pp. 4132-4140.

Meeson, S.; Killingback, A. L. T.; Blott, B. H. (1995): The dependence of EIT images on the assumed initial conductivity distributionl: a study of pelvic imaging. *Phys. Med. Biol.*, vol. 40, pp. 643-657.

Murai, T.; Kagawa, Y. (1985): Electrical impedance computed tomography based on a finite element model. *IEEE Trans. Biomed. Eng.*, vol. 32, pp. 177-184.

Nachman, A. I. (1988): Reconstructions from boundary measurements. *Ann. Math.*, vol. 128, pp. 531-576.

Nachman, A. I. (1996): Global uniqueness for a two-dimensional inverse boundary problem. *Ann. Math.*, vol. 143, pp. 71-96.

Santosa, F.; Vogelius, M.; Xu, J. M. (1999): A non linear elliptic boundary value problem related to corrosion modeling. *Quart. Appl. Math.*, vol. 56, pp. 479-505.

Siltanen, S.; Mueller, J.; Isaacson, D. (2000): An implementation of the reconstruction algorithm of A Nachman for the 2D inverse conductivity problem. *Inverse Problems*, vol. 16, pp. 681-699.

Somersalo, E.; Cheney, M.; Isaacson, D., Isaacson, E. L. (1991): Layer stripping: a direct numerical method for impedance imaging. *Inverse Problems*, vol. 7, pp. 899-926.

Stasiak, M.; Sikora, J.; Filipowicz, S. F.; Nita, K. (2007): Principal component analysis and artificial neural network approach to electrical impedance tomography problems approximated by multi-region boundary element method. *Eng. Anal. Bound. Elem.*, vol. 31, pp. 713-720.

Sylvester, J. (1992): A convergent layer stripping algorithm for radially symmetric impedance tomography problem. *Comm. Partial Diff. Eq.*, vol. 17, pp. 1955-1994.

Sylvester, J.; Uhlmann, G. (1987): A global uniqueness theorem for an inverse boundary value problem. *Ann. Math.*, vol. 125, pp. 153-169.

Wexler, A.; Fry, B.; Neuman, M. R. (1985): Impedance-computed tomography algorithm and system. *Appl. Optics*, vol. 24, pp. 3985-3992.

Yorkey, T.J.; Webster, J. G.; Tompkins, W. J. (1987): Comparing reconstruction algorithms for electrical impedance tomography. *IEEE Trans. Biomed. Eng.*, vol.

34, pp. 843-852.

Zadehkoochak, M.; Hames, T. K.; Blott, B. H.; George, R. F. (1990): A transputer implemented algorithm for electrical impedance tomography. *Clin. Phys. Physiol. Measu.*, vol. 11, pp. 223-230.

Zlochiver, S.; Rosenfeld, M.; Abboud, S. (2003): Induced-current electrical impedance tomography: a 2-D theoretical simulation. *IEEE Trans. Med. Imag.*, vol. 22, pp. 1550-1560.